Journal of Disease Markers

Open Access

Austin Publishing Group

Research Article

Deciphering Regulatory Patterns in a Mouse Model of Hyperoxia-Induced Acute Lung Injury

Yundi Chen[1]; Jinwen Liu[2]; Han Qin[3]; Chunyan Wei[4*]; Xiaolin Hu[2*]

[1]Tongji Medical College, Huazhong University of Science and Technology, Wuhan, China

[2]School of Public Health, Shanghai Jiao Tong University School of Medicine, Shanghai 200025, China

[3]Department of Respiratory and Critical Care Medicine, Kweichow Moutai Hospital, Guizhou, China

[4]Department of Gynecology, Obstetrics and Gynecology Hospital of Fudan University, Shanghai, China

***Corresponding author: Chunyan Wei**

Department of Gynecology, Obstetrics and Gynecology Hospital of Fudan University, 419 Fangxie Rd, Shanghai, China;

Hu Xiaolin, School of Public Health, Shanghai Jiao Tong University School of Medicine, 227 Chongqing South Rd, Shanghai, China.

Email: 16111250010@fudan.edu.cn; 184514@shsmu.edu.cn

Received: April 16, 2024

Accepted: May 23, 2024

Published: May 30, 2024

Abstract

Background: Oxygen therapy is crucial for treating severe ICU patients, but it can lead to hyperoxia and Hyperoxia-induced Acute Lung Injury (HALI), a milder form of Acute Respiratory Distress Syndrome (ARDS). Understanding HALI's underlying mechanism and pathogenesis is essential for improving patient care.

Results: In our study, we established a mouse model of Hyperoxia Acute Lung Injury (HALI) and analyzed gene expression using RNA sequencing. We identified 727 differentially expressed genes, of which 248 were long non-coding RNAs (lncRNAs), and observed significant alternative splicing events. Key findings include the up-regulation and abnormal splicing of genes related to immune response and ferroptosis under hyperoxic conditions. Weighted Gene Co-expression Network Analysis (WGCNA) revealed a distinct cluster of immune response genes that were up-regulated in hyperoxia. Additionally, we constructed a ceRNA network involving 78 mRNAs and 6 lncRNAs, including H19, indicating complex regulatory mechanisms in the pulmonary response to HALI. These results enhance our understanding of HALI's molecular mechanisms and could inform future therapeutic strategies.

Conclusions: Our results provide new insights into the potential mechanisms and underlying pathogenesis in the development of HALI at the post-transcriptional level. The findings of this study encompass driven gene expression patterns, alternative splicing events, and ceRNA networks. These findings may pave the way for advancing therapeutic strategies and reducing the risk associated with oxygen treatment for patients.

Keywords: Hyperoxia Acute Lung Injury; Pathogenesis; RNA-seq; Alternative splicing; ceRNA

Abbreviations: HALI; ARDS; ICU;RNA-seq; ROS; AEC; lncRNAs; WGCNA; ceRNA; mRNA; GO; KEGG; H&E; DEGs; DElncRNAs; AS; A3SS; A5SS; RI; SE; rMATS; GPCRs; miRNAs; TNF; IL; JC

Introduction

Oxygen therapy is one of the most important interventions in treating critically ill patients, including those with COVID-19, a global pandemic. High oxygen concentrations ensure that various organs and tissues of the body obtain sufficient oxygen supply, which is undoubtedly beneficial. However, numerous studies have found that hyperoxia can cause damage to multiple organs such as the lungs, heart and brain, and significantly increase patient mortality. Excessive oxygen therapy can cause Acute Respiratory Distress Syndrome (ARDS), a condition with a high fatality rate. However, only a few effective inventions for ARDS are available to reduce patients' pain, including mechanical ventilation with smaller volume and early prolonged prone-positioning sessions. According to the Berlin definition, ARDS is divided into three kinds: mild, moderate, and severe. Hyperoxia Acute Lung Injury (HALI) is a mild type of ARDS. Mouse exposed to > 95% oxygen can cause HALI and is utilized to study the pathogenesis of HALI. Many mechanisms of HALI have been identified using mouse models, including ferroptosis and immune response [1-4]. Lung cells generate Reactive Oxygen Species (ROS) under high-oxygen conditions [5]. ROS can induce Alveolar Epithelial Cells (AEC) to secrete inflammatory cytokines, thus resulting in damage to pulmonary vascular endothelial cells and AECs, destruction of the alveolar-capillary barrier, formation of lung transparent membranes, and further

Citation: Chen Y, Liu J, Qin H, Wei C, Hu X. Deciphering Regulatory Patterns in a Mouse Model of Hyperoxia-Induced Acute Lung Injury. J Dis Markers. 2024; 9(1): 1060.

development of pulmonary necrosis and fibrosis, and eventually, leading to ARDS.

Our previous studies demonstrated that gene-gene interactions and post-transcriptional regulation are complex in some diseases [6-8]. Numerous studies focus on the destructive role of ROS in cells [9,10], and we realized the mechanisms under the development of HALI are complex, ranging from gene expression pattern, alternative splicing, and ceRNA regulation. So, it's worthy and necessary for underlying the complex interactions and mechanism of regulation of genes involved in the destructive process under ROS and the development of HALI.

With the development of next-generation sequencing technologies, transcriptome-wide analysis, including gene expression and alternative splicing, has been available and affordable. One role of long non-coding RNA (lncRNA) in cells is to act as competing endogenous RNAs (ceRNAs) by sponging miRNA with sequencing match, which inhibits miRNA binding to relevant mRNA and triggers degradation [11]. Increasing evidence suggests that lncRNAs are responsive to ROS and thus contribute to the development of HALI [12].

The present study therefore aimed to underly the potential transcriptional regulation mechanisms and functions of genes for the development of HALI using a hyperoxia-induced mouse model. To this end, a mouse model of HALI was established with hyperoxia condition, and the variation of gene expression pattern was revealed by transcriptome sequencing. Bioinformatics analysis revealed that a total of 727 Differentially Expressed Genes (DEGs), with 248 differentially expressed lncRNAs (DElncRNAs) contained, were involved in the development of HALI.

The biological processes and pathway enrichment showed an up-regulated expression pattern in HALI for genes involved in immune response. Furthermore, the alternative splicing analysis found out some genes were not DE but differentially spliced, such as immune response-related genes (Bax, Spink5, Gpx2, Sox9, IL6, Lif) and ferroptosis-related genes (Gclc, Ftl1). Those results indicate that the hyperoxia condition inflicts negative results not only by influencing gene expression but also by affecting alternative splicing. Finally, a lncRNA-miRNA-mRNA regulatory network was constructed in this study. Our finding offers novel insights into the development of HALI and aids in identifying potential therapeutic targets of HALI, which need to be validated by further experiments.

Results

Generation of Mouse Model of HALI

A model of HALI was developed utilizing twelve C57BL/6J mice. Six mice were randomly selected and exposed to hyperoxia (≥90% oxygen) within an environmentally regulated chamber (25 °C-27 °C, 50-70% humidity) for 72 hours (details in Methods). The remaining six mice were housed in an identical environment with standard oxygen concentration, serving as the control group.

Hematoxylin and Eosin (H&E) staining was conducted to verify the presence of HALI-associated pathological features. As depicted in Figure 1, exposure to hyperoxia resulted in considerable lung injury, characterized by alveolar capillary barrier disruption, pulmonary edema, and infiltration of inflammatory cells. These observations were identical to the clinical observation of the HALI [13], thereby confirming the successful establishment of the HALI murine model.

Identification of Differentially Expressed Genes

The RNA-seq data from six mice with HALI and six control mice were analyzed for a comprehensive identification of genes and isoforms associated with HALI. Gene expression patterns of each sample were quantified with STAR (14), and differential analysis was conducted utilizing DESeq2 [15]. A total of 727 Differentially Expressed Genes (DEGs) were identified (Supplementary Table 1), with genes exhibiting a log2(fold change) > 1.5 or < -1.5 and the p-value < 0.05 considered significantly Differentially Expressed (DEGs). Among these DEGs, 208 were up-regulated in the HALI group (including 43 lncRNAs) and 519 were down-regulated (including 205 lncRNAs) (Fig. 2A, B). Notably, genes associated with HALI were also detected differentially in this study (Supplementary Table 1), such as Bax, Gpx2, Lif, and Ear1, which are related to immune processes. Gclc and Ftl1 are associated with ferroptosis.

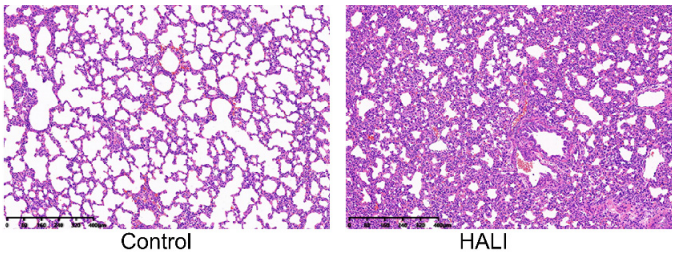

Figure 1: Hematoxylin and Eosin (H&E) staining of the mouse model of HALI. H&E staining of lung tissue in the mouse model of healthy control (left) and HALI (right).

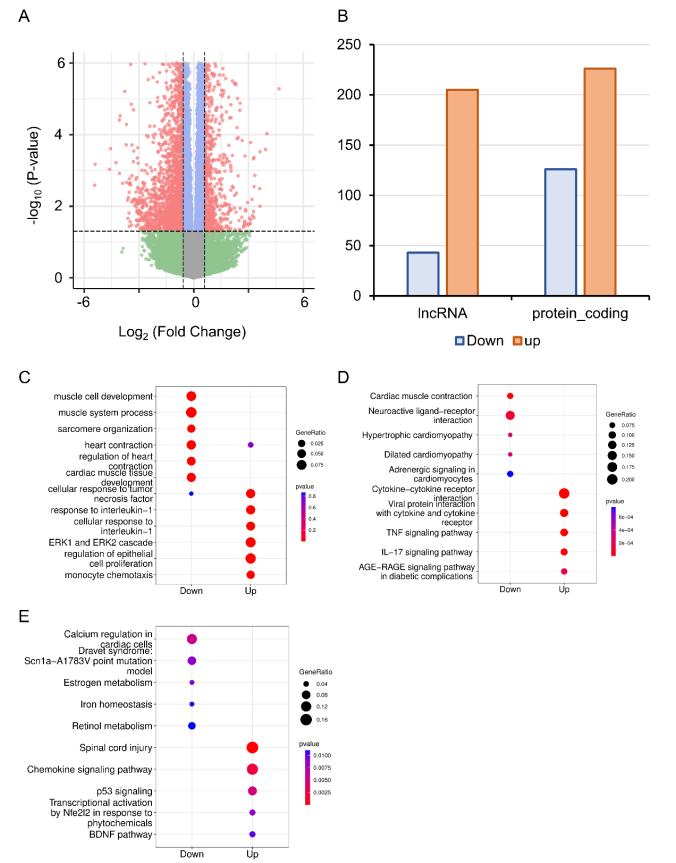

Figure 2: RNA-seq analysis of Differentially Expressed Genes (DEGs) in Hyperoxia-induced Acute Lung Injury (HALI). (A) Volcano plot of DEGs between the model of HALI and the control group. (B) Difference between up-regulated and down-regulated DEGs in mRNA and lncRNA. (C-E) Enrichment analysis for differentially expressed genes, including Gene Ontology (GO) enrichment analysis in biological process (C), Kyoto Encyclopedia of Genes and Genomes (KEGG) pathway enrichment analysis (D), and the enrichment results of WikiPathways (E).

Determination of the Biological Functions of DEGs

To address the biological functions of the DEGs, we conducted enrichment analyses of Gene Ontology (GO) [16], Kyoto Encyclopedia of Genes and Genomes (KEGG) [17], and WikiPathways [18] via the ClusterProfiler [19] package in R (Supplementary Table 2). The up-regulated DEGs in HALI were predominantly enriched in immune response-related functions, such as cellular response to interleukin-1, ERK1 and ERK2 cascade, and monocyte chemotaxis, within the Biological Process (BP) category of GO (Figure 2C). Conversely, downregulated DEGs (including Actn2, Agt, Casq2, Dhrs7c, Drd4, Grin1, Hamp, and so on) in HALI were connected to muscle cell development and myofibril assembly (Figure 2C).

The results of the KEGG pathway enrichment analysis demonstrated that up-regulated DEGs were associated with cytokine-cytokine receptor interactions, Tumor Necrosis Factor (TNF) signaling pathway, and interleukin-17 (IL-17) signaling pathway (Figure 2D). Conversely, down-regulated DEGs were implicated in biological processes such as cardiac muscle contraction, neuroactive ligand-receptor interaction, and dilated cardiomyopathy, among others (Figure 2D).

WikiPathways [18] is an open, continuously updated, and curated pathway database that encompasses 202 pathways for Mus musculus, covering more than 4500 genes (version 20230610). In this study, we utilized this database to augment the pathway resources of the KEGG database. The up-regulated genes were primarily linked to the chemokine signaling pathway, P53 signaling, and Brain-Derived Neurotrophic Factor (BDNF) pathway. In contrast, down-regulated genes were correlated with calcium regulation in cardiac cells, iron homeostasis, and so forth (Figure 2E).

Given that the DEGs participated in multiple biological functions, it was crucial to discern the genes exhibiting distinct patterns to identify the complex biological processes involving these DEGs.

Construction of WGCNA Network

Weighted Gene Co-expression Network Analysis (WGCNA) is a hierarchical clustering approach employed to categorize genes into discrete expression patterns. In the current study, WGCNA discerned five distinct clusters of DEGs by filtering modules with cut-off scores (Figure 3A, Supplementary Table 3). Among these clusters, the grey module encompassed merely four genes, and due to its score falling below the significance threshold, it was filtered out with subsequent analyses. The blue module demonstrated a positive association with the HALI cohort while the turquoise, brown, and yellow modules displayed negative correlations (Figure 3A). The turquoise, blue, and brown modules comprised approximately 200 genes each. The yellow module, on the other hand, contained a minor fraction of DEGs (56 genes) (Figure 3B).

The genes from various modules were subjected to GO and KEGG enrichment analyses. The enrichment results demonstrated that genes in distinct groups were involved in diverse biological processes (Figure 3C, D, Supplementary Table 4). Genes within the blue module were correlated with immune response (e.g., response to interleukin-1, ERK1 and ERK2 cascade, monocyte chemotaxis), which resembled the up-regulated genes' enriched terms in DEG analysis. Genes within the brown module were related to muscle system processes, muscle cell development, myofibril assembly, and so forth. Meanwhile, genes in

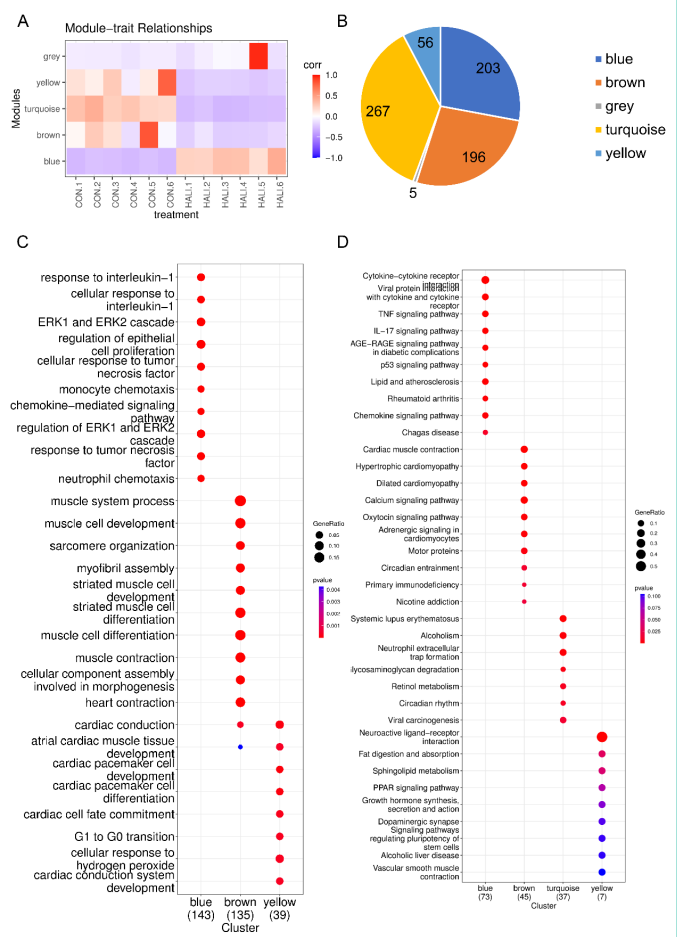

Figure 3: WGCNA of Differentially Expressed Genes (DEGs) (A). Hierarchical clustering heatmap depicting the co-expressed genes in different modules. The rows represent different samples, while the gene expression patterns of the different groups are depicted in separate columns. (B) Number of DEGs in the different groups. Results of (C) GO and (D) KEGG enrichment analysis of the DEGs in the different groups.

the turquoise module were associated with cardiac conduction, cardiac pacemaker cell development, and other relevant processes.

Upon examination of the enrichment analysis, it appears that genes exhibiting down-regulation in response to HALI events can be grouped into two distinct patterns. Conversely, up-regulated genes display a strikingly similar pattern across instances.

Identification of Differential Alternative Splicing

Alternative Splicing (AS) expands the number of proteins and is a key post-transcriptional regulatory mechanism. Therefore, investigating AS events is crucial for understanding the development of HALI. To this end, we employed rMATS to detect five types of AS events: Skipped Exon (SE), Alternative 3' Splicing Sites (A3SS), Alternative 5' Splicing Sites (A5SS), Mutually Exclusive Exons (MXE), and Retained Intron (RI) (20). We considered AS events with a p-value of less than 0.05 to be differentially alternative splicing events (Supplementary Table 5). For specific genes exhibiting multiple splicing events, the AS events with the minimum P-value and higher inclusion level difference were selected as the typical differential AS events (Supplementary Table 6). As depicted in Figure 4A, approximately 10% of AS events were differential. SE was the predominant AS type, followed by MXE, RI, A3SS, and A5SS, which had the fewest differential AS events. Most genes with differential AS exhibited only one type of AS. Notably, only three genes—Gas5, Smox, and Snhg17—

demonstrated all five types of differential AS events (Figure 4B). Gas5, a long non-coding RNA (lncRNA), functions as a competitive endogenous RNA (ceRNA) that sequesters miR429, thereby inhibiting DUSP1 in HALI [21]. Smox expression has been reported to increase under hyperoxia-induced neuronal damage in the retina [22].

Regarding genes not significantly expressed but exhibited differential Alternative Splicing (AS), we juxtaposed our DEGs with differentially AS events (Supplementary Table 7). 159 genes showed differentially expressed but not AS, 1744 genes showed AS but not differentially expressed, and only 5 genes showed both significance in AS events and DE genes (Asns, Lrrc74b, Nr4a1, Slc26a10, Snhg15) (Figure 4C, 4D). Among those five genes, Snhg15 has been implicated in the suppression of cell apoptosis, expression of inflammatory cytokines, and oxidative stress response by up-regulating miR-362-3p expression in IPS-induced vascular endothelial cell [23]. Overexpression of Nr4a1 could reduce the damage of Dex on hypoxia reoxygenation-induced in mouse pulmonary vascular endothelial cells [24].

Alternative Splicing Events Involved in Immune Response and Ferroptosis

Immune response plays a crucial role in the development of HALI [1,3]. Therefore, analyzing alternative splicing events of immune-related genes is of particular interest. To this end, we surveyed a list of immune genes from the Gene Ontology (GO) database (immune system process, GO:0002376), including 2929 genes.

We discovered that 60 genes exhibited differential expressions during the HALI onset (Figure 5A, Supplementary Table 8). By intersecting these results with AS results from rMATS, we identified 1237 events with significant alternative splicing when HALI developed, covering 422 genes. Our findings revealed those immune-related genes underwent alternative splicing during HALI (Figure 5B). Notably, we observed a significant up-regulation of Bax during HALI (Figure 5A), concurrent with significant AS happened to Tmbim6. Given in previous studies that Tmbim6 acts as a suppressor of Bax (25), the abnormal AS of Tmbim6 might account for the up-regulation of Bax. Nearly half of the Alternative Splicing (AS) events were classified as Skipped Exons (SE), while only a small portion of AS events were categorized as Alternative 3' Splicing Sites (A3SS) and Alternative 5' Splicing Sites (A5SS) (Figure 5C). Most genes harbored only one type of AS event; however, some genes exhibited multiple AS types. For example, Adgrf5, a gene associated with airway inflammation and potentially regulating CCL2-mediated inflammation [26], harbored four types of AS events (excluding RI), and another gene, Lilrb4b, featured four types of AS events (excluded MXE) (Figure 5D).

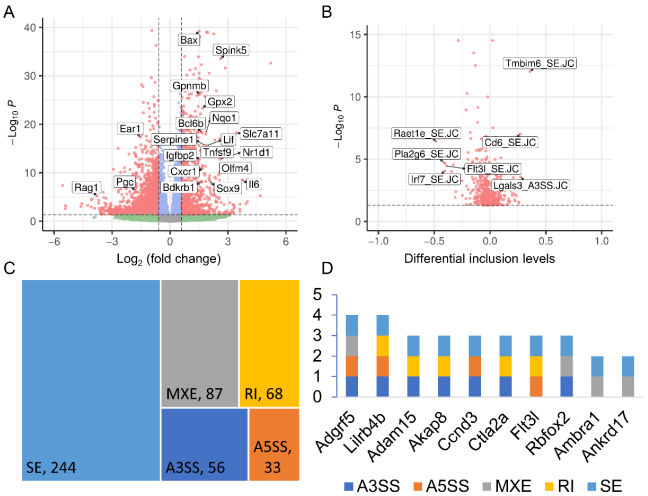

Figure 5: Alternative splicing events in immune response. (A) volcano plot for immune-associated genes. (B) volcano plot for AS events of immune-associated genes. X axis indicated the inclusion level between HALI and control group. Label for the typical gene is a combination of gene symbol, AS type and reads type (JC indicates junction reads only, details described by rMATS). (C) percentage of genes in different AS types. (D) numbers of AS types for typical genes.

In addition to immune response, ferroptosis is one of the key mechanisms in the occurrence of HALI [4]. We retrieved a list of 33 ferroptosis-related genes from the KEGG database (KEGG ID: map04216). A substantial number of these genes exhibited up-regulation in the context of HALI (Figure 6A, Supplementary Table 9), albeit not statistically significant, corroborating previous findings. Intriguingly, several genes demonstrated significant alternative splicing despite the absence of significant differential expressions, such as Gss, Trp53, and Lpcat3 (Figure 6B). This observation underscores the intricate and precise regulatory mechanisms at the transcriptional level.

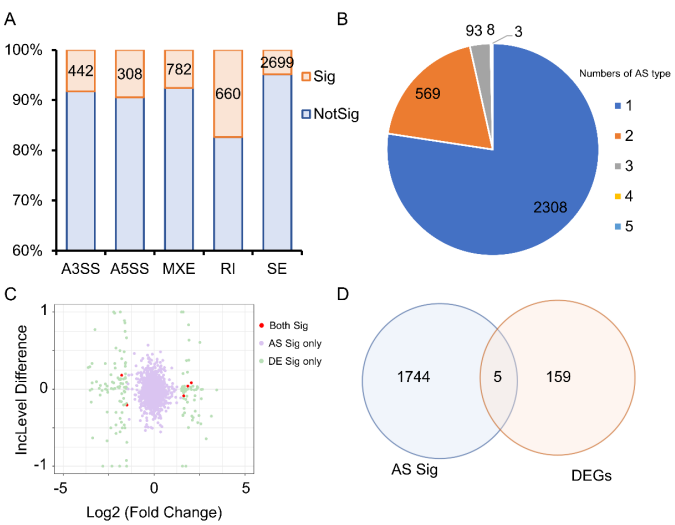

Figure 4: Alternative Splicing (AS) events between HALI and control group. (A) numbers of significant (Sig) and not significant (NotSig) for different types of alternative splicing events. Events with P-value < 0.05 are treated as significant. (B) numbers of types of significant AS events for specific genes. (C) comparison of Differentially Expressed (DE) results and Alternative Splicing (AS) events. The red dot means both significant (Both Sig), the purple dot indicates significant AS but not DE (AS Sig only), and the green dot indicates significant DE but not AS (DE Sig only). (D) the intersection of significant AS (AS Sig) and significant DE (DE Sig).

Identification of miRNA-Target Genes and lncRNAs

248 differentially expressed long non-coding RNAs (lncRNAs) were identified in HALI, including H19 (Supplementary Table 1). This finding prompted us to investigate the potential functions of these lncRNAs. One known function of lncRNAs is their role as molecular sponges for microRNAs (miRNAs), thereby preventing miRNA-mediated mRNA degradation [11]. We obtained miRNA target genes from the multiMiR [27] database and annotated them as either predicted or experimentally validated (Supplementary Table 10). As expected, the majority of lncRNAs harbored one single miRNA targeting a specific mRNA. Notably, Gm10447 harbored 16 miRNAs targeting Cacna2d2, as well as an additional 12 miRNAs targeting another gene, Has2 (Figure 7A).

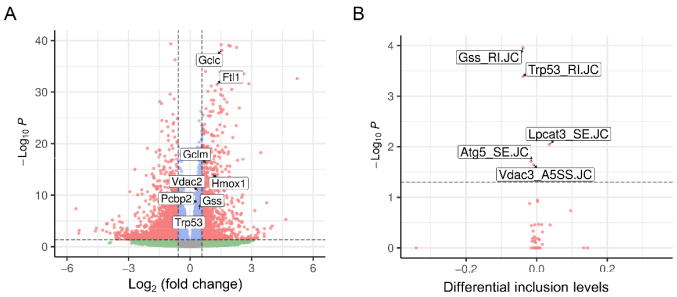

Figure 6: Alternative splicing events involved in ferroptosis. (A) volcano plot for immune-associated genes. (B) volcano plot for AS events for immune-associated genes. X axis indicated the inclusion level between HALI and control group. Label for the typical gene is a combination of gene symbol, AS type and reads type (JC indicates junction reads only, details described by rMATS).

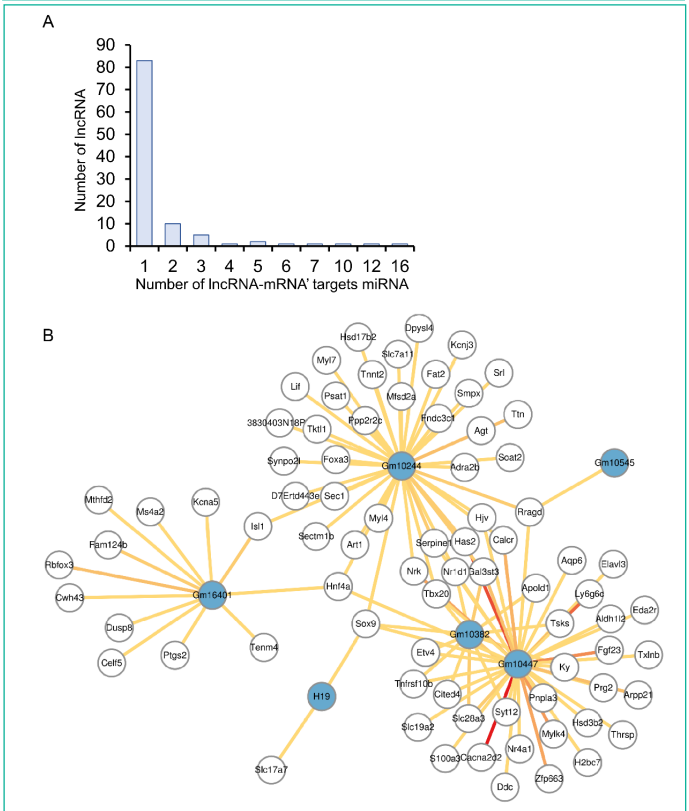

Figure 7: The ceRNA network for key genes. (A). number of miRNAs targeting lncRNA-mRNA pairs. (B) the ceRNA network. The blue dot indicates lncRNA. Deeper red lines indicate the involvement of a higher number of miRNAs.

A comprehensive lncRNA-miRNA-target gene ceRNA network was constructed through the integration of differential analysis and miRNA target investigation (Figure 7B, Supplementary Table 10). Examination of the ceRNA network disclosed potential biological functions of specific lncRNAs, such as H19, GM10382, GM10447, and GM10244. Furthermore, it unveiled potential regulatory interactions of HALI-associated genes, including Slc7a11, Sox9, Mfsd2a, Nr1d1, Ptgs2, and Agt. These genes were implicated in the modulation of cellular ketone metabolic processes (GO:0010565), which is pivotal in the pathogenesis of HALI. Collectively, the ceRNA network analysis elucidated the putative roles of several lncRNAs and genes in the development of HALI, providing valuable insights for future investigations.

Discussion

HALI is a mild form of ARDS as well as a severe outcome of oxygen therapy. Several previous studies have found that mice exposed to >95% oxygen can develop HALI. To investigate the potential mechanisms of HALI development, a mouse model of HALI was established in this study. 12 C57BL/6J mice were purchased, six mice were randomly selected as the HALI group and housed in a hyperoxia (>90% oxygen) chamber for 72 hours, and others were severed as the control group. Then the lung tissues were harvested from these mice and wild-type mice. As depicted in Figure 1, tissues from hyperoxia group exhibited cellular death, a typical phenomenon of HALI observed in humans. These observations validate that the constructed mouse HALI model was suitable for studying the biological processes and transcriptional regulation mechanisms underlying HALI development.

High oxygen concentration is disastrous for lung cells, triggering a series of destructive processes. Initially, lung cells responsively generate Reactive Oxygen Species (ROS) and then cause oxidative stress. Then, alveolar epithelial cells release inflammatory cytokines, inducing neutrophil cells to release cytokines, and then undergo cell death and lung tissue fibrosis, ultimately developing into ARDS. Obviously, this is a destructive process under hyperoxia conditions, and previous studies suggest genetic factors involvement in HALI development [23].

While previous studies focused on genes associated with HALI development at the expression level, the mechanisms underlying post-transcriptional regulation have not been extensively studied. To address the comprehensive mechanisms of HALI development, we performed transcriptome sequencing of 12 mouse lung tissues (6 HALI mouse models and 6 controls).

The hematoxylin and eosin H&E staining results of the present study are highly consistent with the results in previous reports [13], confirming the reliability of our mouse model to investigate the mechanisms underlying gene transcriptional regulation (Figure 1). Then, gene expression differences between the HALI mice and healthy controls were analyzed, with 727 Differentially Expressed Genes (DEGs) identified. Next, WGCNA was employed for clustering the DEGs exhibiting similar expression patterns. A total of five DEG modules were obtained via WGCNA. The grey module, containing only five genes, was filtered out by WGCNA. DEGs in the different modules are involved in completely different biological processes (Figure 3C, D). DEGs in the blue module were associated with immune response, such as response to IL-1, the ERK1 and ERK2 cascade, monocyte chemotaxis, along with regulation of epithelial cell proliferation and the P53 signaling pathway. Immune responses are considered a significant process during the development of HALI, as dying cells can stimulate the release of inflammatory cytokines and trigger innate and/or adaptive immune responses [28,29]. Inflammatory cells such as polymorphonuclear leukocytes generate Reactive Oxygen Species (ROS) that can lead to the death of alveolar epithelial cells [30]. In turn, epithelial cells secrete proinflammatory cytokines which disrupt the alveolar-capillary barrier [5,31]. Treatment with interleukin-1 receptor antagonist reduced other interleukin and cytokine levels downstream of IL-1β signaling, thereby preventing alveolar disruption and airway fibrosis in vivo [32]. DEGs in the brown module were primarily enriched for processes related to muscle cell development, myofibril assembly, and iron homeostasis. This initial observation of genes associated with muscle in lung cells may relate to alveolar septum thickening under hyperoxia conditions (Figure 1) and previous reports of collagen deposition and pulmonary fibrosis in rodents [33]. For example, P2rx2 enriched in those terms was reported to be upregulated under intermittent hypoxia in rat lungs by quantitative real-time PCR [34]. DEGs in the yellow module were associated with G Protein-Coupled Receptors (GPCRs), which have been implicated in neutrophil dysfunc-

tion during sepsis-induced acute respiratory distress syndrome [35], and involvement of downstream GPCR signaling cascades (such as Rho-ROCK, Ras, Akt and NF-kB) in the development of hyperoxia-induced neonatal lung injury [36].

Our previous research has shown the significance of post-transcriptional regulation mechanisms, such as Alternative Splicing (AS) and competitive endogenous RNA (ceRNA) interactions, in the development of various diseases. Many studies have also investigated the roles of those mechanisms in the progression of HALI.

Alternative Splicing (AS) is a key regulatory mechanism that enables limited genes to be translated into numerous proteins. Previous studies have suggested the importance of AS in HALI pathogenesis, with genes involved in mRNA splicing found to be up-regulated under hyperoxia [37]. Other studies have shown that IL-13 selectively stimulates certain VEGF164 isoforms, and the combination of IL-13 and hyperoxia can increase the expression of other VEGF120 and VEGF188 isoforms in HALI [38]. However, a systematic and comprehensive analysis of AS during HALI remains to be conducted. To bridge this gap in knowledge, we conducted a comprehensive analysis of AS during the development of HALI. Our analysis identified a total of 1237 AS events across 422 genes. We also focused on two major processes of HALI pathogenesis: immune response and ferroptosis. Our results revealed that some genes exhibited significant alternative splicing, even if they were not significantly expressed. For example, Cd6 is a lymphocyte surface marker involved in TCR signaling in non-small cell lung cancer [39] and has three isoforms. Additionally, Trp53, a gene encoding tumor protein 53 and involved in ferroptosis, was not significantly expressed in HALI but showed one Retained Intron (RI) event. This gene induces cell cycle arresting, apoptosis, senescence and other processes, and has two isoforms. By analyzing these alternative splicing events, we aim to deepen understanding of the immune response's role in HALI development and potentially identify novel therapeutic targets.

Long non-coding RNAs (lncRNAs) act as competing endogenous RNA (ceRNA) by sponging miRNA, inhibiting the exchange of miRNA binding elements with mRNA. Several studies have shown that abnormal expression of lncRNAs may be associated with the development of HALI [40,41]. For example, gadd7 sponges miR-125a, thus preventing this miRNA from binding to MFN1 [42], and CASC2 ameliorates HALI by sponging miR-144-3p, preventing this miRNA from binding to AQP1 [43]. Those studies highlight the importance of lncRNA in HALI and the potential as biomarkers and therapeutic targets. Our analysis identified 200 differentially expressed lncRNAs involved in HALI development. Combined with the MultiMir database, 148 lncRNA-miRNA-mRNA interactions were found. Among these, we found that lncRNA H19 interacts with Sox9. To be specific, H19 was found to be upregulated in fibroblasts in idiopathic pulmonary fibrosis, and the H19-Sox9 axis was found to contribute to hepatocyte death and liver fibrosis, both of which were observed in HALI [1,44] (Figure 1). However, further studies and experimental validation are necessary to confirm the complex mechanisms of post-transcriptional regulation in HALI development.

Methods

Construction of the Mouse Model

A total of 12 C57BL/6J wild-type mice were purchased from Changsha Tianqin Biotechnology Co., Ltd. Six mice were randomly selected and housed in a hyperoxic chamber maintained at 25-27°C and 50-70% relative humidity. Oxygen flow into the chamber was regulated to keep oxygen levels at ≥90% saturation. Sodium lime was placed inside the chamber to absorb carbon dioxide exhaled by the mice and maintain CO2 levels below 0.5%. Mice were exposed to hyperoxia for 23.5 hours per day. The chamber was open for 0.5 hours daily at scheduled times to provide food, water, and clean bedding.

H&E Staining Procedure

Mice were exposed to 90% percent oxygen for 72 hours in a hyperoxic chamber and euthanized with pentobarbital intraperitoneal injection, finally. Lung tissues were then harvested from hyperoxia-exposed mice and processed into sections on glass slides. The slides were deparaffinized in xylene and rehydrated through immersion in a series of graded alcohols (100%, 90% and 70%). The sections were then stained with hematoxylin for 3 minutes followed by 2 minutes of eosin staining, and rinsed in distilled water. Finally, the sections were dehydrated through another series of graded alcohols (70%, 90% and 100%), cleared in xylene and evaluated for lung injury under the light microscope.

RNA Isolation and Quality Control

Lung tissues were collected from the mice and processed accordingly. Total RNA was extracted using TRIzol reagent (Magen, China) following the manufacturer's instructions. RNA quantity and purity were evaluated spectrophotometrically using a Nanodrop ND-2000 (Thermo Scientific, USA) based on the A260/A280 ratio. RNA integrity was further assessed using an Agilent Bioanalyzer 4150 (Agilent Technologies, CA, USA), and only RNA samples with an RNA integrity number (RIN)≥8 were used for library construction.

Library Preparation for RNA-seq

Library preparation was performed following the Abclonal mRNA-seq Library Preparation Kit (Abclonal, China) protocol. For each sample, 1 μg of total RNA was used to enrich and purify polyadenylated mRNAs using oligo(dT) beads. The purified mRNAs were then reverse transcribed into cDNA using reverse Rnase H and DNA polymerase I. The cDNA libraries were validated for appropriate size distribution using an Agilent Bioanalyzer 4150 (Agilent Technologies, CA, USA). Finally, the libraries were subjected to 150 bp paired-end sequencing on an Illumina NovaSeq 6000 platform.

Quality Control and Read Mapping

The mouse reference genome and gene annotation files (GRCm39, release M32) were downloaded from the GENCODE database [45]. Adapter sequences, low-quality reads (≥20% of bases with Phred score <15), and reads containing >5% ambiguous bases were trimmed using Trim Galore (v0.6.4) [46]. The quality of the trimmed reads was assessed using FastQC (v0.12.0) [47]. The cleaned reads were then aligned to the reference genome using STAR (v2.7.10b) [14] with default parameters. Read counts were derived from the alignments and quantified at the gene level.

Identification of Differentially Expressed Genes

Gene expression for each sample was consolidated using ensemble IDs, and differential expression analysis was executed with DESeq2 (v1.36.0) [15]. Significant differentially expressed

genes were identified based on the following criteria: log2 fold change > 1.5 or < -1.5 and P-values < 0.05. Visualization of differentially expressed genes was accomplished using a volcano plot generated with the ggplot2 package (v3.3.6) [48] and a heatmap created with the ComplexHeatmap package (v2.10.0) [49] in R 4.1.0 [50].

GO, KEGG and WikiPathways Enrichment Analyses

Gene Ontology (GO) [16], KEGG pathway [17], and WikiPathways [18] enrichment analyses were conducted to examine the biological functions of Differentially Expressed Genes (DEGs). These genes were categorized into two groups according to their regulatory directions (Up and Down), based on log2 fold change (log2FC) values. Enrichment analysis was performed and visualized using the ClusterProfiler package (version 4.2.2) [19] in R software (version 4.1.0) [50]. Terms with P-values less than 0.05 were considered significantly enriched.

Construction of WGCNA Network

Differentially expressed genes were clustered into distinct groups using the WGCNA package (v1.70.3) [51] in R, according to their expression patterns. Modules exhibiting a module significance score of < 0.05 were identified as recurrence-associated modules.

Similarly, distinct gene clusters were subjected to GO and KEGG pathway enrichment analysis using the ClusterProfiler package (V4.2.2) [19] to identify various aspects of biological functions. Terms with a P-value < 0.05 were considered significantly enriched.

Identification of Differential Alternative Splicing Events

Splicing is an essential process that determines various cellular fates and directs diverse biological pathways. In this study, we utilized mapped read data from each sample (in BAM format) and combined it with mouse annotation files (in GTF format) as input. We employed rMATS (v3.3.0) [20] to quantify the splicing events for each sample and identify differential alternative splicing events

A statistical summary of alternative splicing for each sample was conducted using the summary.py script from rMATS (v4.1.2) [20]. Differential alternative splicing events with a P-value < 0.05 were considered significant. If a gene exhibited more than one type of alternative splicing, the most significant event was selected for visualization in a volcano plot using ggplot2 (v3.3.6) [48] in R 4.1.0 [50].

Exploring the lncRNA and mRNA Targets of miRNAs

There are lots of tools and databases available for predicting or collecting miRNA-target gene interactions. MultiMir [27] is one of the most comprehensive databases, incorporating both validated miRNA-target interaction databases (miRecords [52], miRTarBase [53], TarBase [54]) and predicted miRNA-target interaction databases (DIANA-MicroT-CDS [55], EIMMo, MicroCosm, miRanda, miRDB, PicTar, PITA, and TargetScan [56]). Moreover, it provides an R package to enable user-friendly downloading of these results. In this study, we utilized MultiMir (version 1.22.0) [27] to query Differentially Expressed Genes (DEGs) and differentially expressed long non-coding RNAs (DElncRNAs) targeting miRNAs, and subsequently saved the obtained results.

Construction of ceRNA Network

According to the ceRNA hypothesis, differentially expressed mRNA (DEmRNA), differentially expressed lncRNA (DElncRNA), and their corresponding targeting miRNAs were collected using the multiMiR (v1.22.0) [27] package in R (v4.1.0) [50]. The lncRNA-miRNA-mRNA ceRNA network was constructed based on these results and visualized using Cytoscape (v3.10) [57].

Author Statements

Ethics Approval and Consent to Participate

The care and use of experimental animals were carried out in accordance with the Directory Proposals and approved by committee of the Ethics Committee of Affiliated Hospital of Zunyi Medical College (ID. Zyfy-an-2023-0047).

Availability of Data and Materials

The datasets generated and analyzed during the current study are available in the GEO database (GSE237260).

Competing Interests

The authors declare that the research was conducted in the absence of any commercial or financial relationships that could be construed as a potential conflict of interest.

Funding

This study was supported by National Natural Science Foundation of China (No. 82303948).

Author Contributions

Y.C., C.W. and X.H. conceived and designed the project. The analyses were performed by X.H. and Y.C. X.H. and C.W. supervised the project. Y.C., S.Q., C.W., X.H. prepared the manuscript. All the author(s) have read and approved the final version of the manuscript.

Acknowledgements

The authors acknowledge the support provided by the Kweichow Moutai Hospital, Shanghai Medical School, Fudan University. Shanghai Jiao Tong University School of Medicine.

References

1. Chen IT, Huang L-T, Chen C-C, Chen C-M. Molecular mechanisms underlying hyperoxia-induced lung fibrosis. Pediatrics & Neonatology. 2022; 63: 109-16.
2. Chen Y, Wei D, Zhao J, Xu X, Chen J. Reduction of hyperoxic acute lung injury in mice by Formononetin. PloS one. 2021; 16: e0245050.
3. Soundararajan R, Hernández-Cuervo H, Stearns TM, Griswold AJ, Patil SS, Fukumoto J, et al. A-Kinase Anchor Protein 1 deficiency causes mitochondrial dysfunction in mouse model of hyperoxia induced acute lung injury. Frontiers in pharmacology. 2022; 13: 980723.
4. Yin X, Zhu G, Wang Q, Fu YD, Wang J, Xu B. Ferroptosis, a new insight into acute lung injury. Frontiers in Pharmacology. 2021; 12: 709538.
5. Dias-Freitas F, Metelo-Coimbra C, Roncon-Albuquerque Jr R. Molecular mechanisms underlying hyperoxia acute lung injury. Respiratory medicine. 2016; 119: 23-8.
6. Hu X, Zou Q, Yao L, Yang X. Survey of the binding preferences of RNA-binding proteins to RNA editing events. Genome Biology. 2022; 23: 1-22.

7. Wei C, Mei J, Tang L, Liu Y, Li D, Li M, et al. 1-Methyl-tryptophan attenuates regulatory T cells differentiation due to the inhibition of estrogen-IDO1-MRC2 axis in endometriosis. Cell death & disease. 2016; 7: e2489-e.

8. Zhang T, Hu X, Yu S, Wei C. Construction of ceRNA network based on RNA-seq for identifying prognostic lncRNA biomarkers in Perthes disease. Frontiers in Genetics. 2023; 14: 1105893.

9. Sies H, Belousov VV, Chandel NS, Davies MJ, Jones DP, Mann GE, et al. Defining roles of specific reactive oxygen species (ROS) in cell biology and physiology. Nature Reviews Molecular Cell Biology. 2022; 23: 499-515.

10. Unsal V, Dalkıran T, Çiçek M, Kölükçü E. The role of natural antioxidants against reactive oxygen species produced by cadmium toxicity: a review. Advanced pharmaceutical bulletin. 2020; 10: 184-202.

11. Salmena L, Poliseno L, Tay Y, Kats L, Pandolfi PP. A ceRNA hypothesis: the Rosetta Stone of a hidden RNA language? Cell. 2011; 146: 353-8.

12. Dutta S, Zhu Y, Han Y, Almuntashiri S, Wang X, Zhang D. Long Noncoding RNA: A Novel Insight into the Pathogenesis of Acute Lung Injury. Journal of Clinical Medicine. 2023; 12: 604.

13. Kallet RH, Matthay MA. Hyperoxic acute lung injury. Respiratory care. 2013; 58: 123-41.

14. Dobin A, Davis CA, Schlesinger F, Drenkow J, Zaleski C, Jha S, et al. STAR: ultrafast universal RNA-seq aligner. Bioinformatics. 2013; 29: 15-21.

15. Love MI, Huber W, Anders S. Moderated estimation of fold change and dispersion for RNA-seq data with DESeq2. Genome biology. 2014; 15: 550.

16. Ashburner M, Ball CA, Blake JA, Botstein D, Butler H, Cherry JM, et al. Gene ontology: tool for the unification of biology. Nature genetics. 2000; 25: 25-9.

17. Kanehisa M, Goto S. KEGG: kyoto encyclopedia of genes and genomes. Nucleic acids research. 2000; 28: 27-30.

18. Slenter DN, Kutmon M, Hanspers K, Riutta A, Windsor J, Nunes N, et al. WikiPathways: a multifaceted pathway database bridging metabolomics to other omics research. Nucleic acids research. 2018; 46: D661-D7.

19. Wu T, Hu E, Xu S, Chen M, Guo P, Dai Z, et al. clusterProfiler 4.0: A universal enrichment tool for interpreting omics data. The Innovation. 2021; 2: 100141.

20. Shen S, Park JW, Lu Z-x, Lin L, Henry MD, Wu YN, et al. rMATS: robust and flexible detection of differential alternative splicing from replicate RNA-Seq data. Proceedings of the National Academy of Sciences. 2014; 111: E5593-E601.

21. Li J, Liu S. LncRNA GAS5 suppresses inflammatory responses and apoptosis of alveolar epithelial cells by targeting miR-429/DUSP1. Experimental and Molecular Pathology. 2020; 113: 104357.

22. Narayanan S, Xu Z, Putluri N, Sreekumar A, Lemtalsi T, Caldwell R, et al. Arginase 2 deficiency reduces hyperoxia-mediated retinal neurodegeneration through the regulation of polyamine metabolism. Cell death & disease. 2014; 5: e1075-e.

23. Liu G, Tian R, Mao H, Ren Y. Effect of lncRNA SNHG15 on LPS-induced vascular endothelial cell apoptosis, inflammatory factor expression and oxidative stress by targeting miR-362-3p. Cellular and Molecular Biology. 2022; 67: 220-7.

24. Dong W, Yang H, Cheng M, Zhang X, Yin J, Zeng Z, et al. Dexmedetomidine alleviates pulmonary ischemia-reperfusion injury through modulating the miR-21-5p/Nr4a1 signaling pathway. Acta Biochimica Polonica. 2020; 67: 521-9.

25. Seitaj B, Liu Q, Parys JB, Methner A, Bultynck G, editors. The function of TMBIM-containing proteins in Ca2+ signaling. BELGIAN SOCIETY OF PHYSIOLOGY AND PHARMACOLOGY, Date: 2018/10/19, Location: Brussels. 2018.

26. Kubo F, Ariestanti DM, Oki S, Fukuzawa T, Demizu R, Sato T, et al. Loss of the adhesion G-protein coupled receptor ADGRF5 in mice induces airway inflammation and the expression of CCL2 in lung endothelial cells. Respiratory Research. 2019; 20: 1-21.

27. Ru Y, Kechris KJ, Tabakoff B, Hoffman P, Radcliffe RA, Bowler R, et al. The multiMiR R package and database: integration of microRNA–target interactions along with their disease and drug associations. Nucleic acids research. 2014; 42: e133-e.

28. Patel VA, Longacre A, Hsiao K, Fan H, Meng F, Mitchell JE, et al. Apoptotic cells, at all stages of the death process, trigger characteristic signaling events that are divergent from and dominant over those triggered by necrotic cells: implications for the delayed clearance model of autoimmunity. Journal of Biological Chemistry. 2006; 281: 4663-70.

29. Hong JY, Kim MN, Kim EG, Lee JW, Kim HR, Kim SY, et al. Clusterin deficiency exacerbates hyperoxia-induced acute lung injury. Cells. 2021; 10: 944.

30. Entezari M, Javdan M, Antoine DJ, Morrow DM, Sitapara RA, Patel V, et al. Inhibition of extracellular HMGB1 attenuates hyperoxia-induced inflammatory acute lung injury. Redox biology. 2014; 2: 314-22.

31. Reddy SP, Hassoun PM, Brower R. Redox imbalance and ventilator-induced lung injury. Antioxidants & redox signaling. 2007; 9: 2003-12.

32. Royce SG, Nold MF, Bui C, Donovan C, Lam M, Lamanna E, et al. Airway remodeling and hyperreactivity in a model of bronchopulmonary dysplasia and their modulation by IL-1 receptor antagonist. American Journal of Respiratory Cell and Molecular Biology. 2016; 55: 858-68.

33. Chen I-T, Huang L-T, Chen C-C, Chen C-M. Molecular mechanisms underlying hyperoxia-induced lung fibrosis. Pediatrics & Neonatology. 2022; 63: 109-116.

34. Wu W, Dave NB, Yu G, Strollo PJ, Kovkarova-Naumovski E, Ryter SW, et al. Network analysis of temporal effects of intermittent and sustained hypoxia on rat lungs. Physiological genomics. 2008; 36: 24-34.

35. Wang Y, Zhu C-l, Li P, Liu Q, Li H-r, Yu C-m, et al. The role of G protein-coupled receptor in neutrophil dysfunction during sepsis-induced acute respiratory distress syndrome. Frontiers in Immunology. 2023; 14: 1112196.

36. Chen X, Walther FJ, Laghmani EH, Hoogeboom AM, Hogen-Esch AC, Van Ark I, et al. Adult lysophosphatidic acid receptor 1-deficient rats with hyperoxia-induced neonatal chronic lung disease are protected against lipopolysaccharide-induced acute lung injury. Frontiers in Physiology. 2017; 8: 155.

37. Tiboldi A, Hunyadi-Gulyas E, Wohlrab P, Schmid JA, Markstaller K, Klein KU, et al. Effects of hyperoxia and hyperoxic oscillations on the proteome of murine lung microvascular endothelium. Antioxidants. 2022; 11: 2349.

38. Corne J, Chupp G, Lee CG, Homer RJ, Zhu Z, Chen Q, et al. IL-13 stimulates vascular endothelial cell growth factor and protects against hyperoxic acute lung injury. The Journal of clinical investigation. 2000; 106: 783-91.

39. Moreno-Manuel A, Jantus-Lewintre E, Simões I, Aranda F, Calabuig-Fariñas S, Carreras E, et al. CD5 and CD6 as immunoregulatory biomarkers in non-small cell lung cancer. Translational Lung Cancer Research. 2020; 9: 1074-1083.

40. Wu Y, Zhang Z, Li J, Zhong H, Yuan R, Deng Z, et al. Mechanism of Adipose-Derived Mesenchymal Stem Cell-Derived Extracellular Vesicles Carrying miR-21-5p in Hyperoxia-Induced Lung Injury. Stem Cell Reviews and Reports. 2022; 18: 1007-24.

41. Chen C, He Y, Feng Y, Hong W, Luo G, Ye Z. Long non-coding RNA review and implications in acute lung inflammation. Life Sciences. 2021; 269: 119044.

42. Liu G, Mei H, Chen M, Qin S, Li K, Zhang W, et al. Protective effect of agmatine against hyperoxia-induced acute lung injury via regulating lncRNA gadd7. Biochemical and Biophysical Research Communications. 2019; 516: 68-74.

43. Li H, Shi H, Gao M, Ma N, Sun R. Long non-coding RNA CASC2 improved acute lung injury by regulating miR-144-3p/AQP1 axis to reduce lung epithelial cell apoptosis. Cell & Bioscience. 2018; 8: 15.

44. Chen I-T, Huang L-T, Chen C-C, Chen C-M. Molecular mechanisms underlying hyperoxia-induced lung fibrosis. Pediatrics & Neonatology. 2022; 63: 109-16.

45. Frankish A, Diekhans M, Jungreis I, Lagarde J, Loveland JE, Mudge JM, et al. GENCODE 2021. Nucleic acids research. 2021; 49: D916-D23.

46. Krueger F. Trim Galore!: A wrapper around Cutadapt and FastQC to consistently apply adapter and quality trimming to FastQ files, with extra functionality for RRBS data. Babraham Institute. 2015.

47. Andrews S. FastQC: a quality control tool for high throughput sequence data. Babraham Bioinformatics, Babraham Institute, Cambridge, United Kingdom. 2010.

48. Wickham H. ggplot2. Wiley interdisciplinary reviews: computational statistics. 2011; 3: 180-5.

49. Gu Z, Eils R, Schlesner M. Complex heatmaps reveal patterns and correlations in multidimensional genomic data. Bioinformatics. 2016; 32: 2847-9.

50. Ihaka R, Gentleman R. R: a language for data analysis and graphics. Journal of computational and graphical statistics. 1996; 5: 299-314.

51. Langfelder P, Horvath S. WGCNA: an R package for weighted correlation network analysis. BMC bioinformatics. 2008; 9: 559.

52. Xiao F, Zuo Z, Cai G, Kang S, Gao X, Li T. miRecords: an integrated resource for microRNA–target interactions. Nucleic acids research. 2009; 37: D105-D10.

53. Huang H-Y, Lin Y-C-D, Li J, Huang K-Y, Shrestha S, Hong H-C, et al. miRTarBase 2020: updates to the experimentally validated microRNA–target interaction database. Nucleic acids research. 2020; 48: D148-D54.

54. Sethupathy P, Corda B, Hatzigeorgiou AG. TarBase: A comprehensive database of experimentally supported animal microRNA targets. Rna. 2006; 12: 192-7.

55. Paraskevopoulou MD, Georgakilas G, Kostoulas N, Vlachos IS, Vergoulis T, Reczko M, et al. DIANA-microT web server v5. 0: service integration into miRNA functional analysis workflows. Nucleic acids research. 2013; 41: W169-W73.

56. McGeary SE, Lin KS, Shi CY, Pham TM, Bisaria N, Kelley GM, et al. The biochemical basis of microRNA targeting efficacy. Science. 2019; 366: eaav1741.

57. Shannon P, Markiel A, Ozier O, Baliga NS, Wang JT, Ramage D, et al. Cytoscape: a software environment for integrated models of biomolecular interaction networks. Genome research. 2003; 13: 2498-504.